



Drop of pressure behavior of open-cell aluminum foams at high pressure flow

M. F. Azamar^{a*} • I. A. Figueroa^a • G. González^a • I. Alfonso^b

^aInstituto de Investigaciones en Materiales, Universidad Nacional Autónoma de México, Ciudad de México, México

^bInstituto de Investigaciones en Materiales, Unidad Morelia, Universidad Nacional Autónoma de México, Campus Morelia, Morelia, México

Received 10 23 2020; accepted 04 22 2021

Available 12 31 2021

Abstract: Open-cell aluminum foams were produced by the replication technique in three different pore sizes, ranging from 0.71 to 4.75 mm. The manufactured specimens were physically characterized, determining their porosity, relative density, pores per inch and interconnection windows density. A new experimental design is proposed in order to assess the drop of pressure behavior resulting from the injection of gasoline additive at increasing high pressure intervals, ranging from 1.38 to 172.37 MPa (200 to 25,000 psi), reproducing the tests at room temperature and 200 °C. The regime governing the flow through the investigated samples was determined as a function of flowrate and the foams physical properties. The structural capacity of open-cell Al foams to conduct highly pressurized flow was evaluated by means of compression tests. It was found that at room temperature, the drop of pressure behavior is strongly associated to physical parameters, whilst at 200 °C, dimensional and geometrical properties are negligible. In addition, in this investigation, it is presumed that the studied foams have the structural capacity to conduct fluids at critical conditions of pressure and temperature.

Keywords: Open-cell aluminum foam, pore size, porosity, high pressure flow, drop of pressure behavior

*Corresponding author.

E-mail address: iafigueroa@unam.mx(I. A. Figueroa).

Peer Review under the responsibility of Universidad Nacional Autónoma de México.

1. Introduction

A metallic foam is a porous medium consisting of a solid metallic matrix with fluid-filled or un-filled pores, distributed throughout its structure. These can be open- or closed-cell according to the physical pore-pore interconnection (Gibson & Ashby, 1997; Liu & Chen, 2014). Depending on the desired structural characteristics and mechanical properties for a specific application, there exist different methods for metallic foams fabrication, some of them are the powder metallurgy, metal deposition and the liquid-state processes. The powder metallurgy process consists of heating and pressing metallic particles until these are compacted into one piece (Banhart, 2000; García-Moreno, 2016). This process allows to control porosity and particle size, but the resulting material exhibits poor mechanical properties, e.g., strength and plastic collapse stress, in comparison with other methods. Metal deposition consists of depositing metallic particles in a polymeric foam, then the polymeric structure is removed, and the remaining metallic particles are sintered (Liu & Chen, 2014). Samples produced by this technique exhibit high sample reproducibility in terms of physical and mechanical properties. Liquid-state processes include, mainly, the replication technique and blowing foaming agent methods. The former is widely used to produce open-cell foams, whilst the latter allows producing closed-cell foams. Samples obtained by both processes have shown excellent mechanical properties (Despois et al., 2007; Luna et al., 2014; Osorio-Hernández et al., 2014; Shi et al., 2017; Trinidad et al., 2014; Velasco-Castro et al., 2018).

Recently, it has been studied and proposed an unconventional technique to produce metallic foams, with no need of foaming agents or space holders. This method consists of the formation of an icosahedral-quasicrystalline phase as an out of equilibrium condition in the Al-Fe-Cu system, subjecting the material to heat treatments. This was called the “In-Situ” foaming method, which allows controlling porosity and pore size by means of adjusting the heat treatment parameters, i.e., temperature and time. This process could be cataloged as an unconventional technique, since at the beginning, the porosity was considered as an unwanted defect (Dubois, 2012; Suarez et al., 2014; Besser & Eisenhammer, 1997).

Nowadays, open-cell aluminum (Al) foams are the most common produced and commercialized kind of metallic foams. Due to the properties of Al as base metal, in addition to the porous interconnected structure, open-cell Al foams can be used in sandwich panels for energy absorption and sound dissipation, in construction as lightweight structures, in chemistry as carriers for catalyst and in hydraulic applications for gases or liquids conduction, heat transfer and filtering (Banhart, 2001; Lefebvre et al., 2008; San Marchi & Mortensen,

2002). The potential uses of open-cell Al foams in hydraulic applications have earned relevance, since this material offers the chance of transport a fluid while this is cooled or heated in its way. A precise description of fluid flow behavior in porous Al is essential to the successful design and operation of projects focused on fluids conduction. Thus, the permeability behavior of open-cell Al foams has been thoroughly explored and well-described within a limited range of flow conditions.

Permeability can be defined as the ability of a material to conduct fluids through its interconnected pores (Tiab & Donaldson, 2012). Its magnitude depends on the physical and structural properties of the medium, such as effective porosity and shape, size, distribution, and pores physical interconnection. There exist different models to study permeability, supported by diverse conditions of porous medium, flow and interaction between the sample surface and the fluid flowing. The most extensively employed model is the Darcy's law (Otaru, 2020; Pal et al., 2006; Tiab & Donaldson, 2012), which idealizes the fluid as incompressible (for liquids) and considers that this does not react with the porous surface, that the porous medium is homogeneous and continuous and that the flow is linear and isothermal. According to Darcy's law, written in Eq. 1, the pressure gradient ($\frac{dP}{dx}$) for a flow through a porous medium is linearly proportional to the product of the fluid velocity (superficial velocity, v) and the dynamic viscosity (μ), and inversely proportional to the permeability coefficient (κ) (Boomsma & Poulikakos, 2002).

$$-\frac{dP}{dx} = \frac{\mu}{\kappa} v \quad (1)$$

Darcy's law describes the phenomenon of fluid flow in porous media, assuming that the inertial forces and the friction between the surface and the fluid are negligible. As the pressure gradient refers to the drop of pressure (ΔP) per unit length (L) and the fluid velocity is the flowrate (Q) per unit area (A), Eq. 1 can be solved for κ as follows:

$$\kappa = \frac{\mu L Q}{\Delta P A} \quad (2)$$

Eq. 2 is well-known as the reduced Darcy's law (RDL) and is valid within a limited range of low flow velocities (Zeng & Crigg, 2006). If the fluid flows at high velocity, the flow in porous media migrates from the Darcy regime to the Forchheimer (non-Darcy) regime, where form drag and inertial forces start to be important and the energy dissipation becomes the sum of viscous and form drag (Dukhan & Ali, 2012). As the fluid velocity increases, RDL fails to describe accurately the permeability coefficient, owing that the linear correlation between the pressure gradient and the fluid velocity disappears. The Forchheimer equation considers the microscopic inertial effect and captures the impact of the force exerted by any solid

surface on the flowing fluid and its resultant effect on the drop of pressure as a second order term (Otaru et al., 2018), modifying Eq. 1 as follows:

$$-\frac{dP}{dx} = \frac{\mu}{\kappa} v + \beta \rho v^2 \quad (3)$$

where β is the non-Darcy coefficient (form drag), ρ is the fluid density and v^2 is the square of the superficial velocity. Contrary to the occurred within the Darcy regime, the Forchheimer effect causes non-linearity between the pressure gradient and the superficial velocity.

The exact beginning of the Forchheimer regime is controversial and has been broadly discussed. Zeng and Crigg (2006) detailed the employed criteria to discern between Darcy and non-Darcy flow. An adjusted Reynolds number (Re) using the mean pore diameter instead of the conduit diameter (D_p), shown in Eq. 4, is a dimensionless alternative criterion to predict the flow behavior through porous media.

$$Re = \frac{\rho D_p v}{\mu} \quad (4)$$

According to Chilton and Colburn (1931), the non-Darcy flow starts at a Re value in the range of 40-80. Blick and Civan (1988) suggested a Re of 100 as a transitional point, below this value, the flow is within Darcy regime whilst above 100 the non-Darcy effect should be considered.

Research concerning the drop of pressure measurements of open-cell Al foams have been previously reported. Boomsma and Poulikakos (2002), Despois and Mortensen (2005), Dukhan (2012), Dukhan et al. (2014), Fernández-Morales et al. (2017) and Otaru et al. (2018) measured the drop of pressure resulting from the injection of diverse fluids through Al foams, aiming to study their permeability and flow behavior. The consensus among all these investigations is the inverse correlation between the value of κ and the drop of pressure, ΔP , as well as the influence on the flow behavior of geometrical and physical parameters, such as pores density (pores per inch, PPI), pore size, porosity, and pore-pore interconnections (windows). Dietrich (2012) determined a correlation for estimating the drop of pressure of single-phase flow inside ceramic sponges using air as testing fluid, extrapolating the obtained data to metal sponges based on geometrical parameters. Mancin et al. (2010) analyzed experimentally and theoretically, the pressure losses during air flow in aluminum foams with different physical properties. Nevertheless, the drop of pressure behavior (DPB) at high flow pressures (>3.45 MPa or 500 psi) and at temperature higher than room temperature is yet unexplored. Proper knowledge of DPB at critical conditions might give way to expand the functional applicability of porous Al.

This paper proposes a new experimental design to analyze DPB when one single phase fluid is injected into open-cell Al foams at increasing pressure intervals, reaching pressure values up to 172.37 MPa (25,000 psi). The investigated foams were manufactured by the replication technique (Luna et al., 2014; Osorio-Hernández et al., 2014; Trinidad et al., 2014) in three different pore sizes. Flow tests were conducted at room temperature and 200 °C, in order to observe the effect of temperature on DPB. The correlation with PPI, pore size, porosity and pore-pore interconnections were also assessed as well as the structural integrity of the Al foams after high pressure flow test (HPFT). The relevance of this investigation is that Al foams performance at these extremely high flow conditions has never been reported before, thus, the results presented in this work could be of interest, for instance, for the energy industry in oil/gas extraction and transportation.

2. Materials and methods

2.1. Fabrication of Al foams

The foams were produced by the infiltration of molten Al with a sodium chloride (NaCl) preform, under an inert argon (Ar) controlled atmosphere. The preform was obtained by sieving NaCl irregular particles in three different size intervals, in order to produce pores of: (A) 0.71 to 1.00 mm, (B) 2.00 to 2.38 mm and (C) 3.35 to 4.75 mm (Fig. 1).



Figure 1. Employed NaCl beads for preform (a) 0.71 to 1.00 mm, (b) 2.00 to 2.38 mm and (c) 3.35 to 4.75 mm.

The experimental setup, for manufacturing Al foams, consisted of a resistance furnace, a cylindrical steel crucible and a valves system with a pressure regulator connected to a

mechanical vacuum pump and an Ar tank. The steps of the process are shown in Fig.2. It can be observed that an Al cylindrical ingot, of commercial purity, was placed on top of the NaCl perform into the crucible (Fig. 2a). Then, the crucible was sealed using graphite O-rings on top and bottom. The system was purged three times, suctioning the air with the mechanical pump to produce a vacuum of 10^{-3} Torr (Fig. 2b). After that, argon (Ar) was introduced to start the melting process (Fig. 2c). The crucible was placed into the furnace at a working temperature of 770-780 °C, which is above the Al melting point (~660 °C) and below the one of NaCl (~800 °C). At this temperature, the metal load was melted under an Ar atmosphere at a controlled pressure of 0.5 kg cm⁻² (P_m) for 60-70 minutes (Fig. 2d). Afterward, the solid NaCl was infiltrated with the molten Al by increasing the Ar pressure (P_i) for 20-30 minutes (Fig. 2e) at pressures of 2, 1.65 and 1.25 kg cm⁻² for pores A, B and C, respectively. Finally, the crucible was extracted from the furnace and placed over a copper (Cu) block to control the metal solidification from bottom to top, thereby inducing the formation of the shrinkage outside the foam volume (Fig. 2f). The composite material (Al-NaCl) was retired from the crucible and machined into cylinders of 5 cm in length and 3.81 cm in diameter, according to testing cell dimensions. The NaCl perform was leached in distilled water by means of an ultrasonic shower, remaining only the porous Al.

2.2. Structural characterization

All produced samples were physically and geometrically characterized. PPI was determined as the number of pores in one linear inch. The pore wall thickness (t_{wall}) refers to the average of several aleatory measurements on each tested foam of the distance between two pores. The density (ρ) of each sample was calculated from measurements of its volume and weight. The relative density was determined as the ratio between the foam density and the bulk density of the metallic matrix material (ρ / ρ_{Al}). The foams porosity (Φ) was obtained according to Eq. 5:

$$\Phi = \frac{V_S - V_{Al}}{V_S} \quad (5)$$

where V_S is the volume of the sample (57 cm³) and V_{Al} is the volume occupied by the Al (solid volume). Based on the Al density ($\rho_{Al} = 2.71$ g cm⁻³), the porosity was estimated, obtaining V_{Al} with the weight of the foams. Then, by means of a helium (He) pycnometer, the real value of V_{Al} was measured and the porosity was likewise obtained with Eq. 5. Finally, one sample of each pore size was taken and machined into eight slices of 0.5 cm in length and 5 cm in diameter from bottom to top, as sketched in Fig. 3. The volumetric (Φ_{vol}) and superficial porosity (Φ_{sup}) of each slice was measured with the aim of observing the porosity along the axial axis of the foams. The

superficial porosity evaluation was carried out by means of the commercial image analysis software (Image J).

2.3. Fluid injection tests

The HPFT was conducted at room temperature and 200 °C, using the pore-permeameter shown in Fig. 4 and gasoline additive as testing fluid. The pore-permeameter consists of a fluid storage tank (Fig. 4a), a mechanical pump (Fig. 4b), a hydraulic press (Fig. 4c), a testing cell (Fig. 4d) inside which the testing section is (Fig. 4e) and an exhaust tank (Fig. 4f). The beforementioned components are coupled with a set of pipelines and valves to transport fluid and control its entrance to each section. The internal pipeline diameter is 0.45 cm, whereas the diameter of the testing section is 3.81 cm. Moreover, the entire experimental setup was computer-controlled.

Firstly, the Al foam sample is mounted into the testing section, using two Teflon/copper gaskets on the bottom and top to properly seal the cell and guarantee the sample confinement. The test starts with the mechanical pump moving the testing fluid from the storage tank to the hydraulic press. Once the latter is full, its valve is closed (Fig. 4g). Then, whilst the testing cell valve is open (Fig. 4h) and the exhaust tank valve is closed (Fig. 4i), the hydraulic press injects the gasoline additive toward the testing cell at preset increasing pressure intervals, ranging from 1.38 to 172.37 MPa (200 to 25,000 psi) with increments of 6.89 MPa (1,000 psi) in each test, i.e., 1.38-6.89, 1.38-13.78, etc., this in order to find out the critical hydrodynamic pressure that can be supported by the Al foams without severe physical damage. The pressure at the inlet and outlet of the sample was measured with two pressure gauges connected to the entrance (Fig. 4j) and exit (Fig. 4k) of the testing section, capturing one value per second. Once the highest value of the preset pressure interval is reached, the exhaust tank valve is opened, and the fluid is expelled from the system.

The fluid injection was upward with regards to the testing section, at a preset flowrate (Q) of 7 cm³ s⁻¹. The cell temperature was measured with a resistance temperature detector (Fig. 4l). It is worth highlight that the analysis temperature acts into the testing section, therefore, the gasoline additive will not necessarily attain this temperature, as each test lasts between 10-20 s.

The structural integrity of open-cell Al foams after HPFT was assessed by generating the stress-strain curves of tested samples by means of compression tests, using a universal mechanical testing machine Instron 1125-5500R, at a crosshead speed of 0.5 mm min⁻¹ and a maximum load of 9,980 kgf (97.870 kN).

The dynamic viscosity, μ , of the gasoline additive was measured using a parallel plate rheometer, at shear rates ($\dot{\gamma}$) ranging from 10 to 1,500 s⁻¹. The rheology tests were conducted at room temperature and 200 °C.

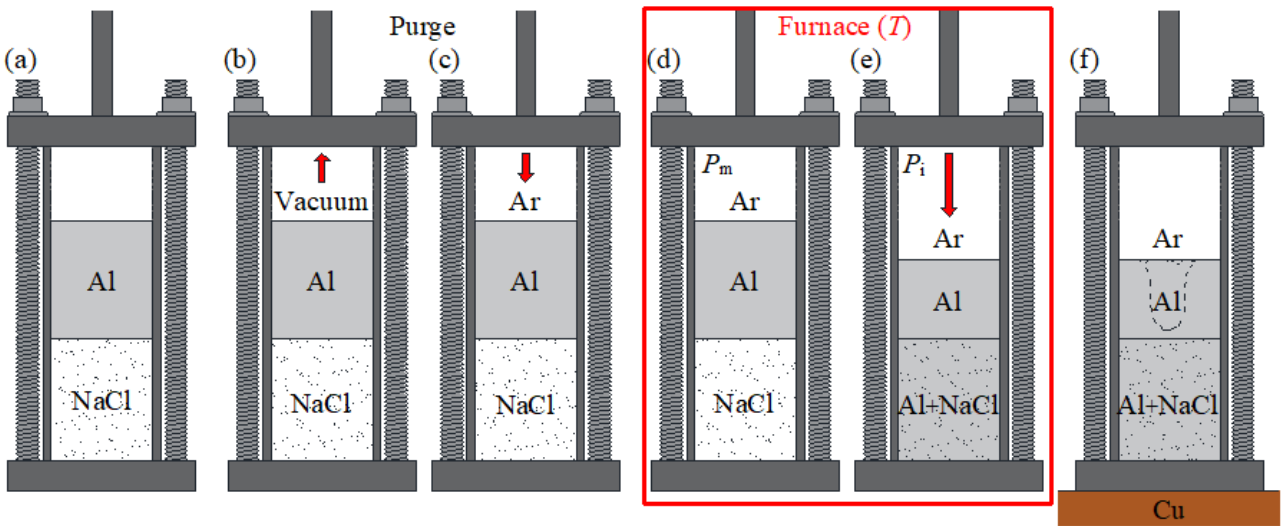


Figure 2. Steps for Al foams production: (a) assembly, (b) vacuum, (c) Ar supply, (d) Al melting, (e) Al infiltration and (f) Al solidification.

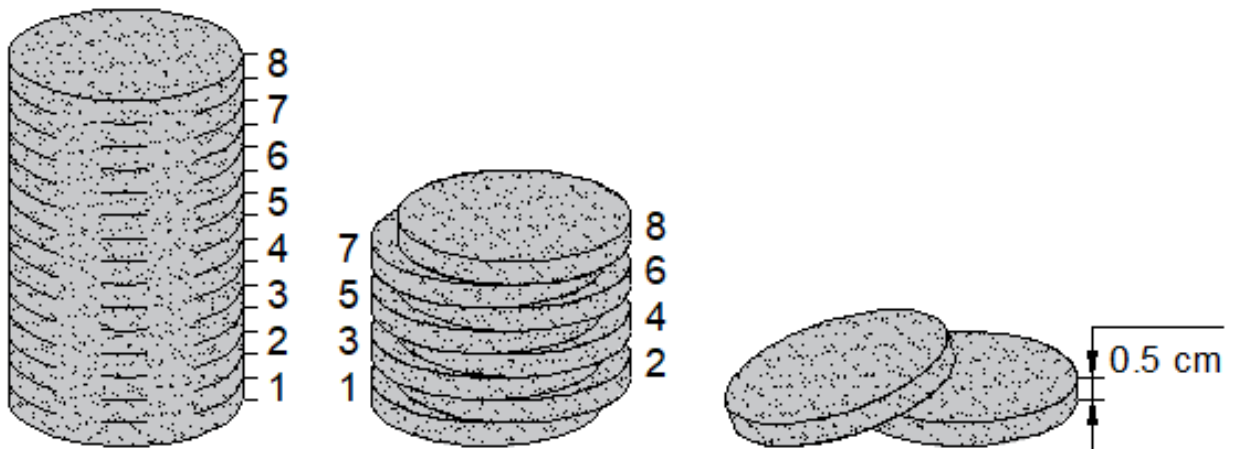


Figure 3. Sketch of the machined slices for porosity analysis along the axial axis of open-cell Al foams.

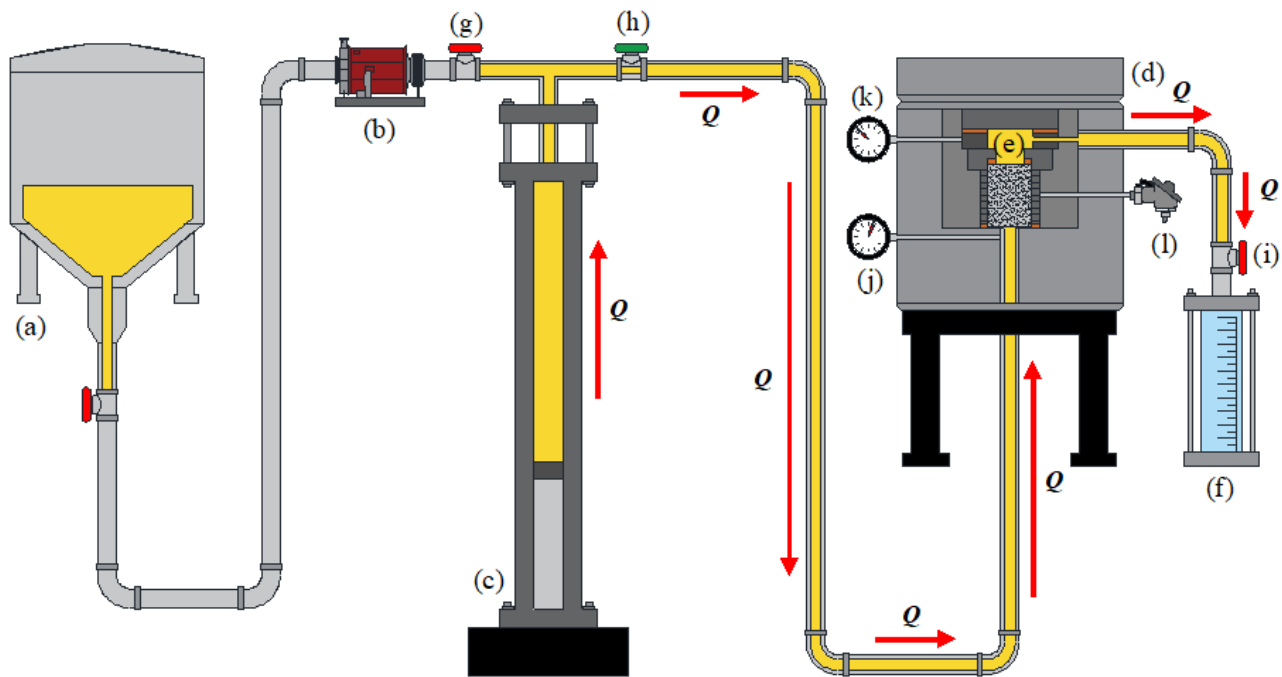


Figure 4. Diagram of the pore-permeameter: (a) testing fluid storage tank, (b) mechanical pump, (c) hydraulic press, (d) testing cell, (e) testing section, (f) exhaust tank, (g, h, i) valves, (j, k) pressure gauges and (l) resistance temperature detector.

3. Results and discussion

3.1. Production of Al foams and physical characterization

Fig. 5 shows the foams produced for HPFT. It can be appreciated the absence of defects, such as lack of infiltration or NaCl particles embedded, forming a composite material. The resulting size difference among pores A (Fig. 5a), B (Fig. 5b) and C (Fig. 5c) is reasonably significant, as expected. In the top view of the samples, shown in Fig. 5d, it is observed that the pores geometry is highly irregular, which is a consequence of the used NaCl particles. Nevertheless, the pores distribution observed over the sample flat surface is rather homogeneous, despite its stochastic nature.

Table 1 presents the physical and structural properties of Al foams. The measured weight, m , and solid volume, V_{Al} , were rather similar for all the investigated samples, with a data dispersion within $\pm 1\%$. Therefore, the relative density, ρ^* , and porosity, Φ , were practically the same with a typical value of 0.38 and 62%, respectively. In contrast, the pores per inch, PPI, and pore wall thickness, t_{wall} , exhibited the highest variation among all the studied foams, as expected, due to their strong relationship with pore size.

Fig. 6 shows the volumetric and superficial porosities, Φ_{Vol} and Φ_{Sup} , as a function of the sample height, Δh . Porosity values

corresponding to the slices from the same foam described by almost horizontal lines in these plots, suggesting the uniformity of the pore's distribution along the axial axis (vertical direction) of samples, and demonstrating the non-existence of a porosity gradient. The volumetric porosity (Fig. 6a) remained at $62\% \pm 2\%$ for all analyzed slices, whereas superficial porosity (Fig. 6b) for pore A tended to be significantly lower ($34\% \pm 4\%$) when compared to that for pores B and C ($55\% \pm 5\%$). The beforementioned allows theorizing the absence of a direct correlation between both porosities. It is worth noting that this porous homogeneity does not necessarily mean an isotropic behavior of the flow through Al foams.

3.2. Drop of pressure and flow analysis

The fluid velocity, v , was calculated according to the methodology described by Despois and Mortensen (2005), assuming spherical pores and using data from Table 1 with a flowrate of $7 \text{ cm}^3 \text{ s}^{-1}$. The modified Re for porous media was calculated according to Eq. 4, using the values of density ($\rho = 0.78 \text{ g cm}^{-3}$) and dynamic viscosity ($\mu = 0.0023 \text{ Pa}\cdot\text{s}$) of the gasoline additive at room temperature. Re for fluid flow into the pore-permeameter pipeline was also calculated, as reference. Results are compiled in Table 2.

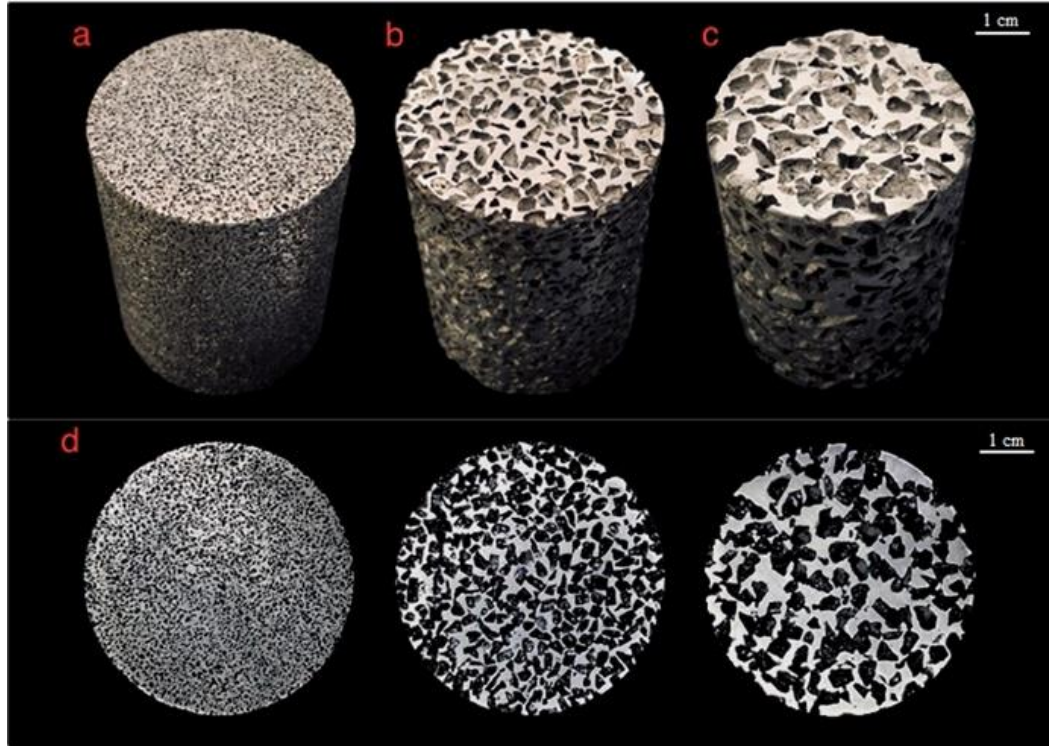


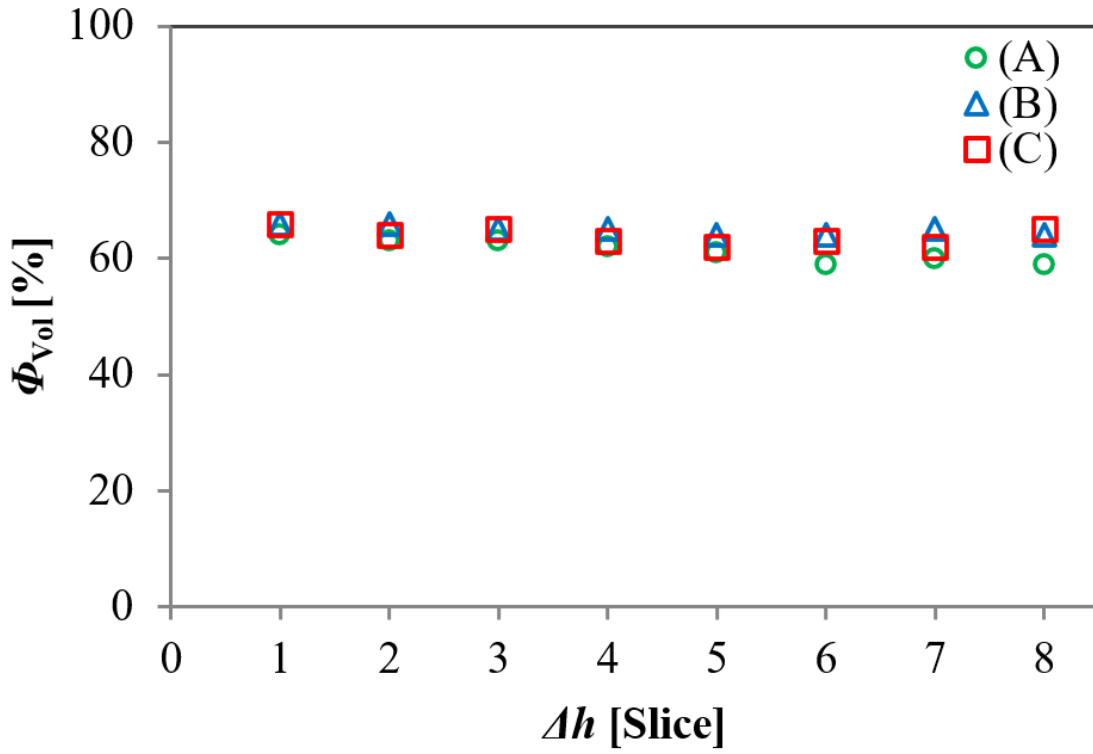
Figure 5. Al foams produced with pore sizes of: (a) (A) 0.71 to 1.00 mm, (b) (B) 2.00 to 2.38 mm, (c) (C) 3.35 to 4.75 mm and (d) Al foams observed from the top view.

Table 1. Experimentally determined structural and physical properties of the produced Al foams.

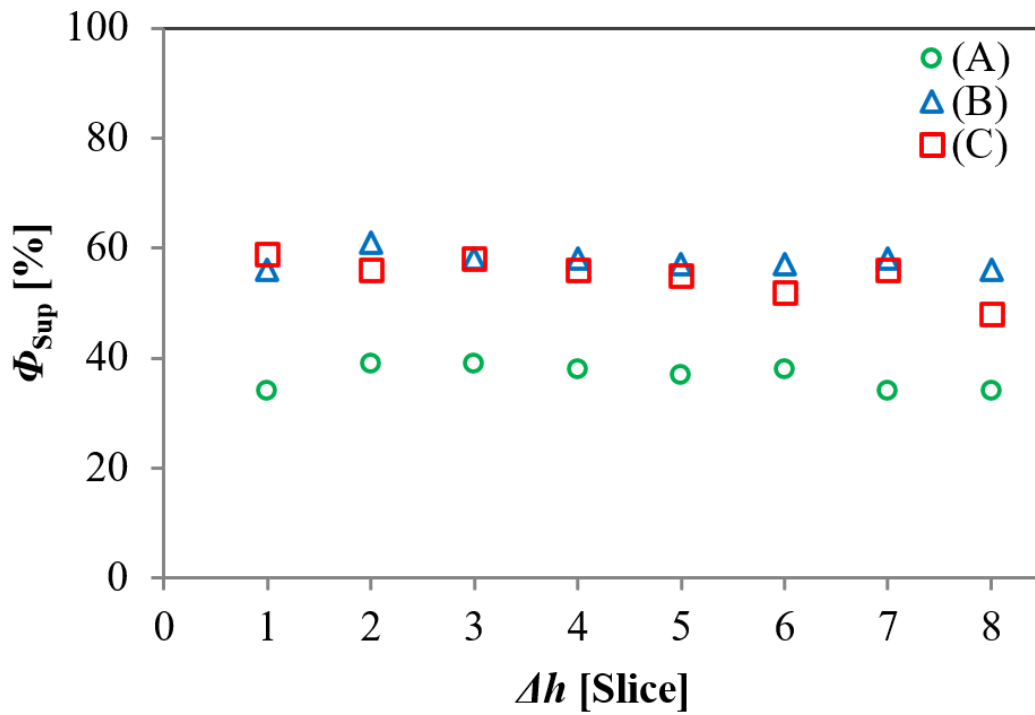
Pore size	m [g]	V_{Al} [cm ³]		PPI	t_{wall} [mm]	ρ [g cm ⁻³]	ρ^*	Φ [%]	
		Estimated	Measured					Estimated	Measured
(A) 0.71 - 1.00 mm	59.10	21.81	21.76	29	0.55	1.04	0.38	62	62
(B) 2.00 - 2.38 mm	58.40	21.55	21.44	12	1.19	1.02	0.38	62	62
(C) 3.35 - 4.75 mm	58.50	21.59	21.52	7	1.88	1.03	0.38	62	62

Table 2. Fluid velocity and modified Re for all flow conditions.

Pore size	D_p [mm]	v [cm s ⁻¹]	Re	Flow regime
(A)	0.71	1644.27	3921.61	Forchheimer
	1.00	828.88	2784.34	Forchheimer
(B)	2.00	207.22	1392.17	Forchheimer
	2.38	146.33	1169.89	Forchheimer
(C)	3.35	73.86	831.15	Forchheimer
	4.75	36.74	586.18	Forchheimer
Pipeline	4.50	44.30	669.58	Laminar



(a)



(b)

Figure 6. Porosity behavior along the axial axis of Al foams, (a) volumetric porosity and (b) superficial porosity.

The lower obtained Re , corresponding to the upper size limit of the larger pore, is remarkably higher than the criterion values established to discern between flow regimes. Thus, the flow through all studied foams is undeniably within Forchheimer regime. On the other hand, the flow through the pipeline, before the fluid entrance into porous media, is within the laminar regime ($Re < 2,000$), which is sort of analog to Darcy flow. This fact highlights the effect of open-cell Al foams irregular structure ("bottleneck") and tortuosity dictating flow behavior, as the fluid velocities for the pore diameter of 4.75 mm and that of the pore permeameter conduit are rather similar, but the flow regimes are completely different. From Table 2, it is also noted that the fluid velocity is strongly dependent on the pore size magnitude, as the velocity estimated for the smallest pore diameter (0.71 mm, $1,644.27 \text{ cm s}^{-1}$) is almost 45 times bigger than the value of v for the largest pore ($C = 4.75 \text{ mm}$, 36.74 cm s^{-1}).

Fig. 7 shows the drop of pressure as a function of the pressure at the outlet of the sample when HPFT were conducted at room temperature (Fig. 7a) and $200 \text{ }^\circ\text{C}$ (Fig. 7b). The flow rate started to drop when the hydrodynamic pressure exerted by the fluid approached the upper value defined for the pressure interval, i.e., 137.90 for 1.38 to 137.90 MPa, 172.37 for 1.38 to 172.37 MPa, as a relaxation response due to the proximity, observing this flow behavior in all tested samples. For analysis purposes, only drop of pressure values corresponding to a steady flow of $7 \pm 0.2 \text{ cm}^3 \text{ s}^{-1}$ were taken. Thus, the maximum pressure attained with the aforementioned flow is closely 103.42 MPa (15,000 psi). Nonetheless, the fluid pressure of 172.37 MPa (25,000 psi) was reached at flow rates between 0 to $1 \text{ cm}^3 \text{ s}^{-1}$. Pressure losses associated with the confining wall effect were ignored, as all HPFT tested samples had the same dimensions (Dukhan & Ali, 2012).

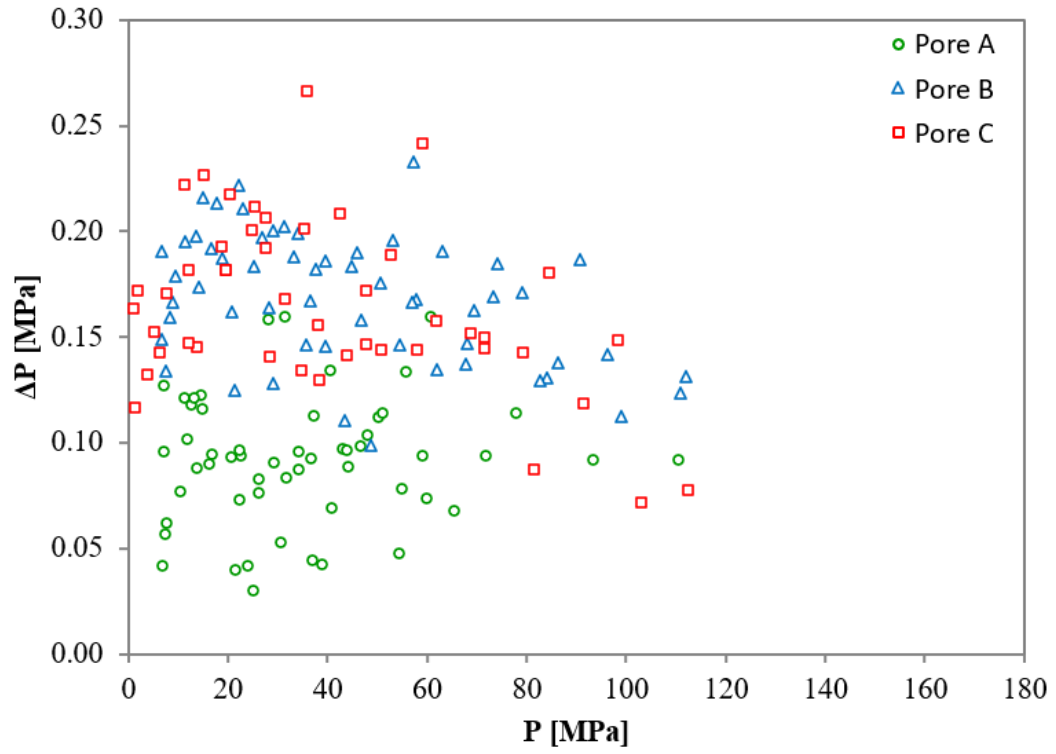
At room temperature is noticeable a tendency to present lower pressure losses for pore A regard to pores B and C, contrary to the expected. Otaru et al. (2018) demonstrated the key role within the Forchheimer regime of the windows that interconnect the pores, based on their size and alignment, finding that lower pressure differences are associated with larger windows. Fig. 8 shows some scanning electronic microscopy (SEM) images for the HPFT tested samples, where the windows (bottlenecks) can be appreciated, being marked with red arrows. An amount of 13, 6 and 3 windows were counted for pores A, B and C, respectively, within a 10.8 mm^2 area. The windows density is noteworthy higher as the pore size decreases, although larger pores compensate this with larger windows. Due to the pore shape irregularity, the mean diameter and window connectivity area are difficult to determine and would not be representative values; therefore, this investigation avoids their calculation. It is worth mentioning that the windows density is directly linked to the

pore's density (PPI in Table 1), prevailing a similar amount ratio among the investigated pores. As the porosity for all investigated foams was $62\% \pm 2\%$ regardless of pore size, these unexpected outcomes are attributed to windows density, being apparently more decisive the amount of these structures than their sizes.

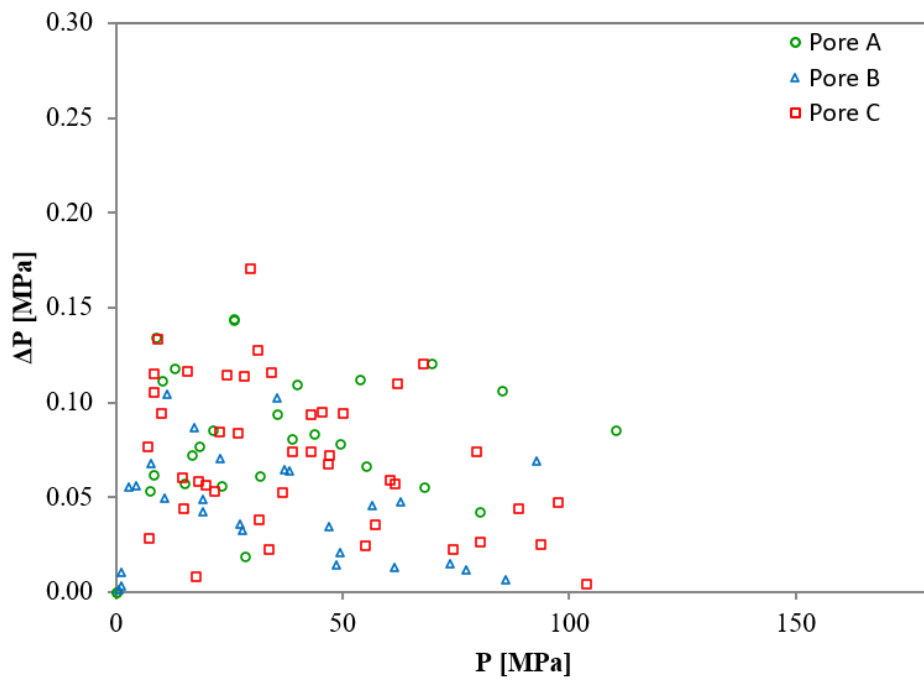
At $200 \text{ }^\circ\text{C}$, it is not observed a clear trend associated with the pore size, relating this performance to the temperature effect. However, either at room temperature or $200 \text{ }^\circ\text{C}$, a slight tendency of ΔP to decrease as the pressure at the outlet of the samples increases is appreciated. The data scattering and non-linearity of ΔP as the injection pressure increases could be attributed to drag variations, resulting from the friction between the Al foam surface and the fluid flowing at extremely high velocities, turbulent in nature.

Fig. 9 shows the flowrate ($Q = 7 \pm 0.2 \text{ cm}^3 \text{ s}^{-1}$) as a function of the drop of pressure, at room temperature (Fig. 9a) and $200 \text{ }^\circ\text{C}$ (Fig. 9b). The drop of pressure outcomes surprisingly fell into a range of values and not into a single value. In the same way that in the drop of pressure vs. pressure plots (Fig. 7), this behavior might be attributed to the drag variations linked to the achieved fluid velocity. At room temperature, the range of pressure losses has lower values for the smallest pore, A, when compared to the larger ones, B and C, with the data dispersion being rather similar for A and B. The inverse correlation between the fluid velocity and flow pressure is well-known, i.e., as the fluid velocity increases, the pressure exerted by the fluid decreases. Thus, according to data from Table 2, pore A foams would have lower flow resistance than that for pores B and C. On the other hand, at $200 \text{ }^\circ\text{C}$, the pressure losses are practically within the same range of values regardless of the pore size, which leads to suggest that, at higher temperatures, the influence of dimensional parameters becomes negligible, at least for open-cell Al foams (presumably).

Fig. 10 shows the flowrate as a function of the drop of pressure plots at both temperature conditions for pores A (Fig. 10a), B (Fig. 10b) and C (Fig. 10c). For the medium and largest pores (B and C, respectively) the pressure losses clearly display an inverse correlation with temperature, i.e., as the temperature increases, the drop of pressure decreases. Considering that the flow behavior through porous media does not depend exclusively on the conduction channels geometry but also on the properties of testing fluid flowing, the performance of the latter should also be evaluated. Fig. 11 shows the dynamic viscosity, μ , as a function of the shear rate, γ , at 25 (room temperature), 40, 60, 100 and $200 \text{ }^\circ\text{C}$. From the rheology analysis is observed that the magnitude of the dynamic viscosity is directly affected by temperature, because of the weakening of friction among the microlayers of the fluid. Thus, it is possible to deduce that when HPFT are conducted at a temperature higher than $25 \text{ }^\circ\text{C}$, the DPB will be different from that expected at room temperature for the same foam.



(a)



(b)

Figure 7. Drop of pressure as a function of the pressure at the outlet of the sample at (a) room temperature and (b) 200 °C.

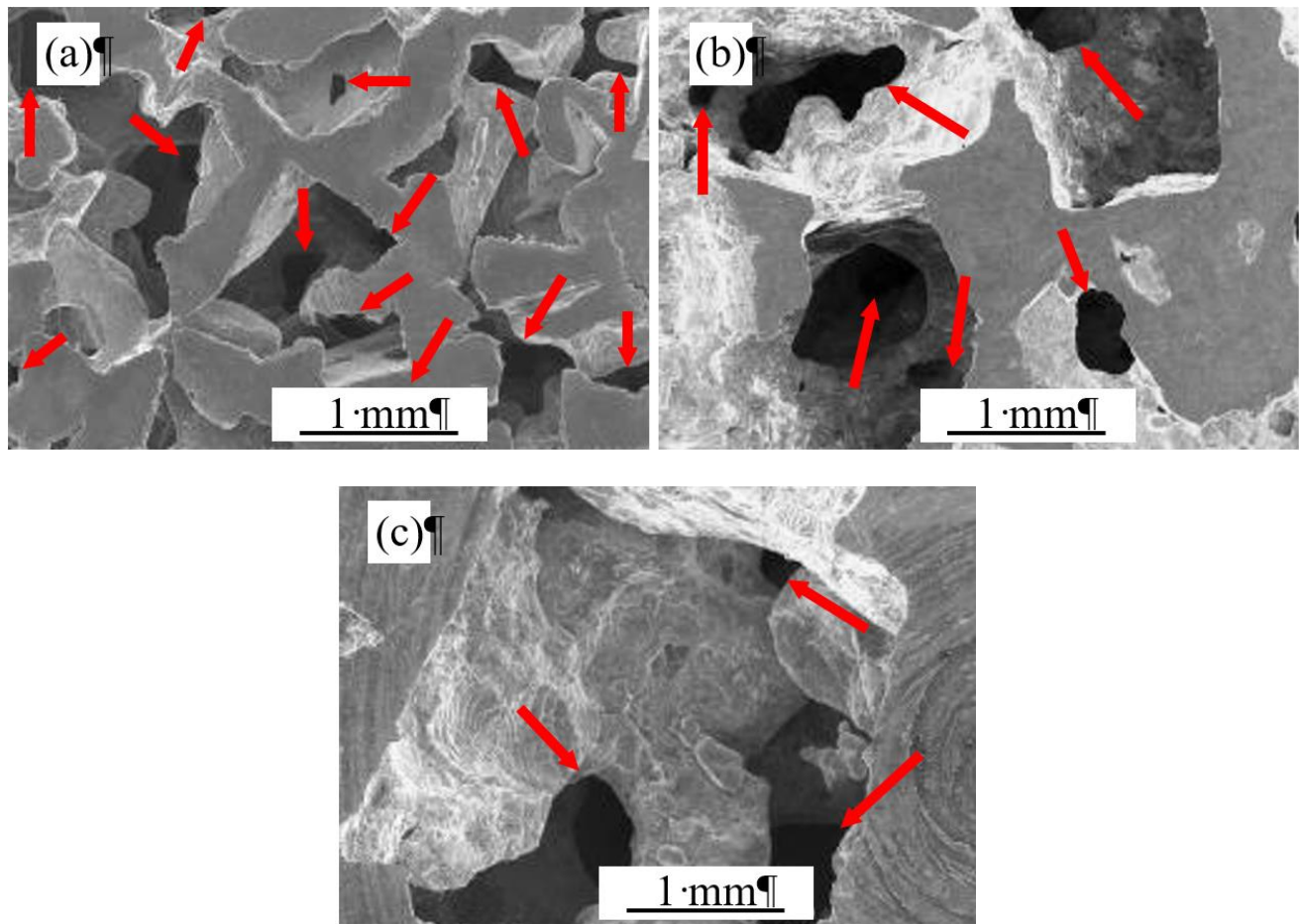


Figure 8. SEM images of the windows resulting from the pore-pore interconnections of the produced Al foams (a) (A) 0.71 to 1.00 mm, (b) (B) 2.00 to 2.38 mm and (c) (C) 3.35 to 4.75 mm.

The first term at the right in Eqs. 1 and 3 refers to the pressure gradient (drop of pressure per unit length) required to overcome the viscous resistance (Zeng & Crigg, 2006). Therefore, a reduction of the viscous forces (μ) means a reduction of the resistance to flow, resulting in a lower drop of pressure values. The outcomes shown in Fig. 10b and Fig. 10c could also be attributed to the decrease of the gasoline additive density. As the flow is within Forchheimer regime, a lower density will have repercussions on inertial forces, represented by ρ in the second term at the right in Eq. 3, thereby having repercussions on the pressure gradient.

The relationship between the drop of pressure and temperature for pore A is not as clear as for pores B and C. The smallest value of ΔP in Fig. 10a corresponds to HPFT at 200 °C, whilst the largest ΔP value corresponds to HPFT at room temperature. Thus, the influence of temperature on DPB for pore C is subtle but exists.

3.3. Structural integrity assessment

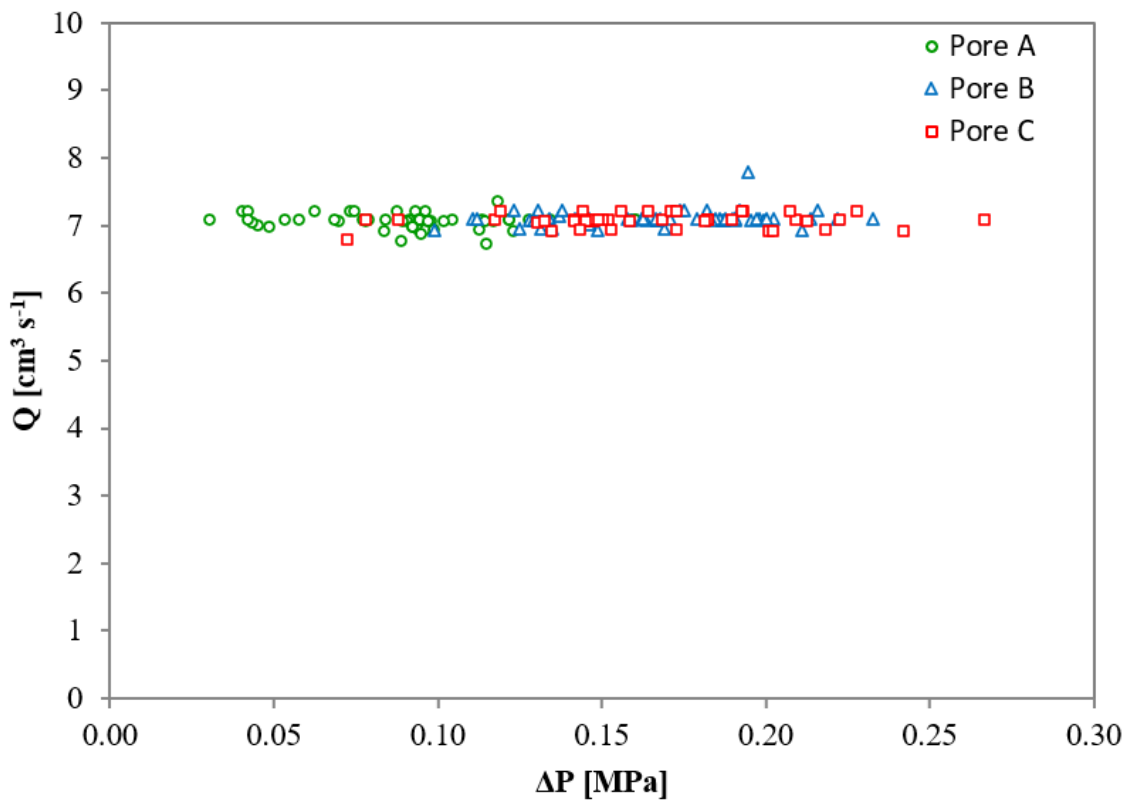
Starting from the fact that Al has high strength and toughness, in addition to its ductile mechanical behavior, it could be assumed that an Al based porous structure has the capacity to conduct highly pressurized flow without important physical damage, at least at room temperature. Nevertheless, an increase of the testing temperature might have repercussions on the foam's metallic matrix, e.g., microstructurally changes associated to diffusion effects, in detriment of the material performance. Fig. 12 shows a foam with pore C (Fig. 12a) before and after (Fig. 12b) HPFT at 200 °C. It can be externally appreciated that the foam structure did not collapse as a consequence of the critical testing conditions. The stains along the length of the sample are the only visual difference in the aspect of the foam before and after the HPFT. These stains are the result of the contact between the sample external hot surface and the burned gasoline additive. Fig. 13 shows the stress-strain diagram generated from the sample shown in Fig. 12.

and its respective non-HPFT tested reference. The HPFT curve showed the expected compressive behavior for open-cell Al foams, without observing an early structural collapse. The energy absorption capacity, defined as the area under the stress-strain curve, was calculated for the HPFT sample and its reference, finding that both samples absorbed 3.41 MJ m⁻³ for 38% strain. Thus, it is assumed that the analyzed samples were not structurally damaged because of the extremely high hydrodynamic pressure at 200 °C.

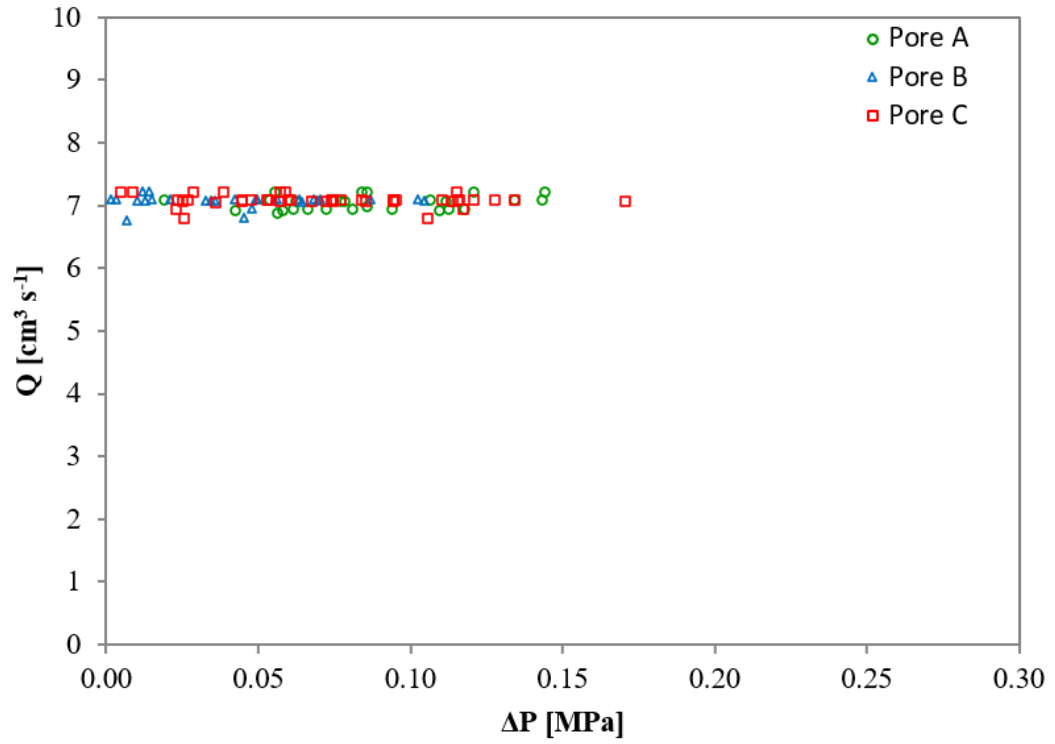
The fact that open-cell Al foams present a rigid structure and are capable of supporting high pressure flow without deformation or significant physical alterations allows to reject any possible experimental errors, thereby reducing uncertainty. Grossmann et al. (2018) studied the water permeability of fibrous membranes for biomedical applications, suggesting that a nonlinear behavior of the permeability with increasing pressure might be caused by

the deformation of the nonwovens like a compression of the membrane or at least a rearrangement of the nanofibers, because of the 120 mmHg (0.016 MPa or 2.3 psi) hydraulic pressure.

In order to contextualize the physical dimensions or technological implications of using 172.37 MPa, this pressure is equal to 1,700 times the atmospheric pressure at the sea level, 17.5 times the hydrostatic pressure exerted by the water column over the shell of a nuclear submarine at 1,000 m deep and 1.5 times the water column at the Mariana trench, the deepest known point on earth (Fig. 14). From this figure, it can be observed that pressure of 172.37 MPa is exceptionally high. Therefore, the results of this research are important since metallic foams have never been investigated nor proposed for industries that may need to conduct fluids at high pressure, such as energy industries. Thus, the results presented in this research give way to a new engineering application of these materials.

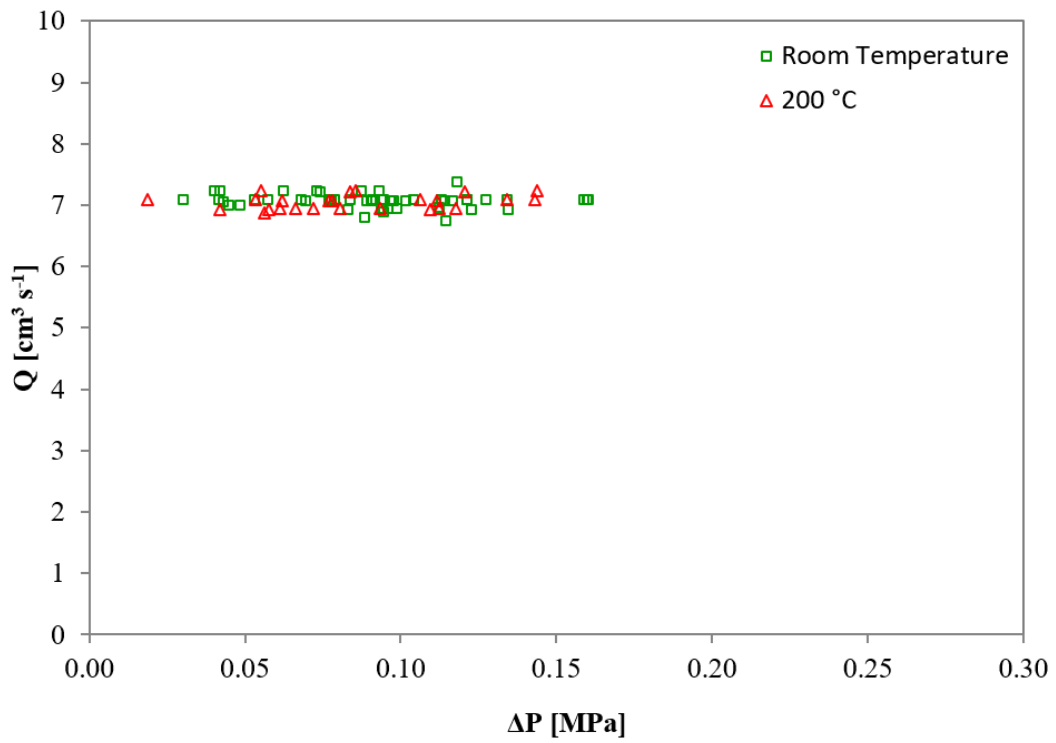


(a)

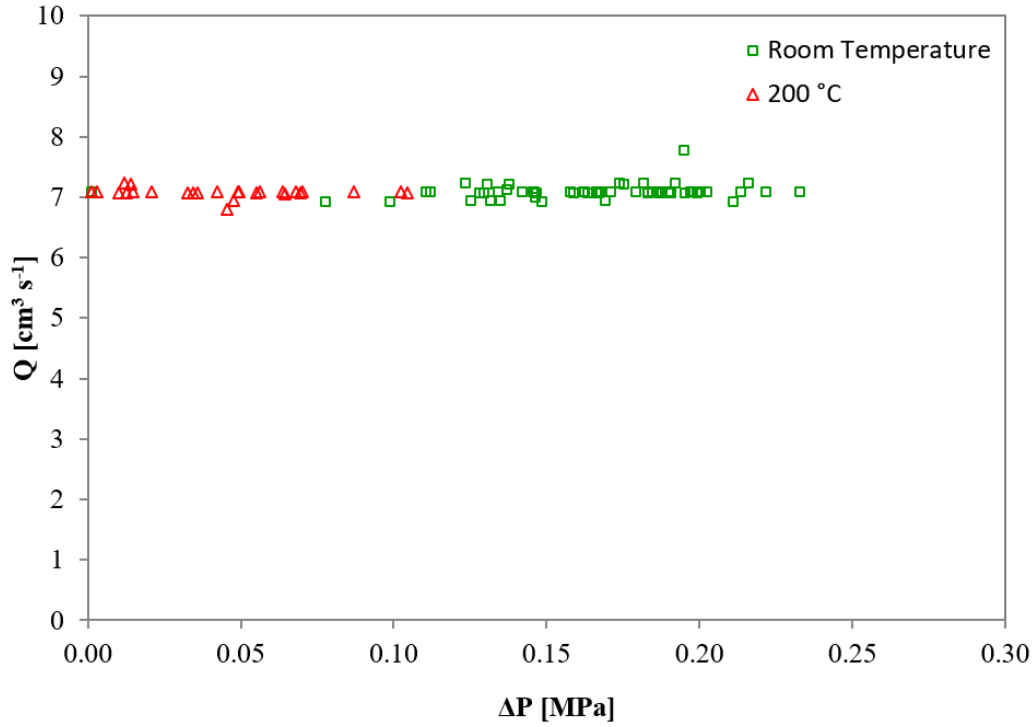


(b)

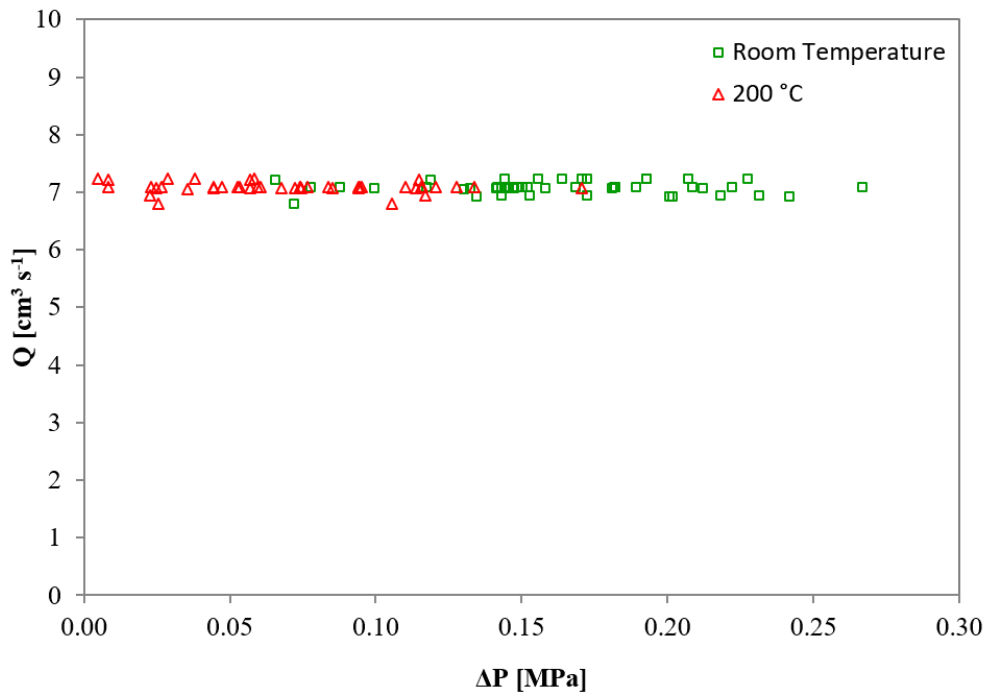
Figure 9. Flowrate as a function of the drop of pressure at (a) room temperature and (b) 200 °C.



(a)



(b)



(c)

Figure 10. Flowrate as a function of the drop of pressure at room temperature and 200 °C for pore (a) (A) 0.71 to 1.00 mm, (b) (B) 2.00 to 2.38 mm and (c) (C) 3.35 to 4.75 mm.

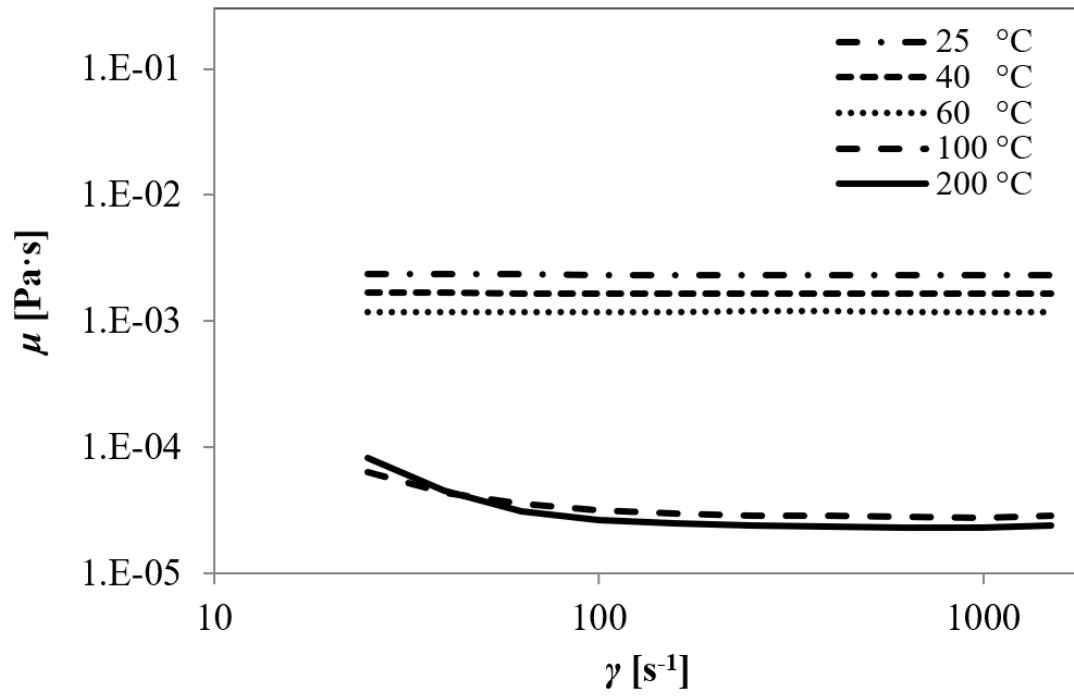


Figure 11. Gasoline additive rheology results at different testing temperatures.

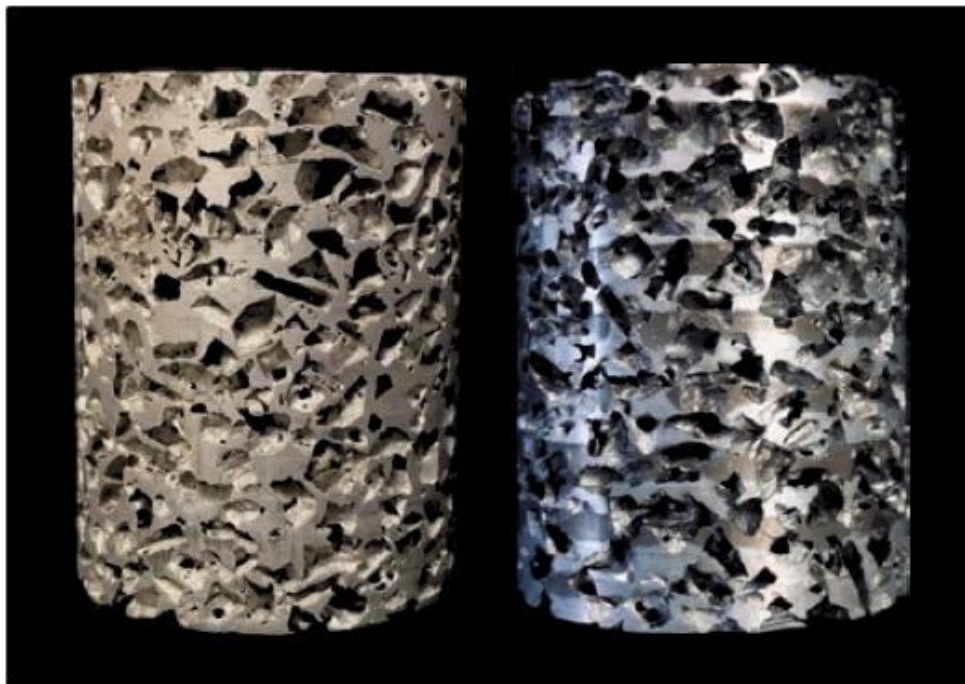


Figure 12. Al foam of pore (C)(a) before and (b) after HPFT at 200 °C.

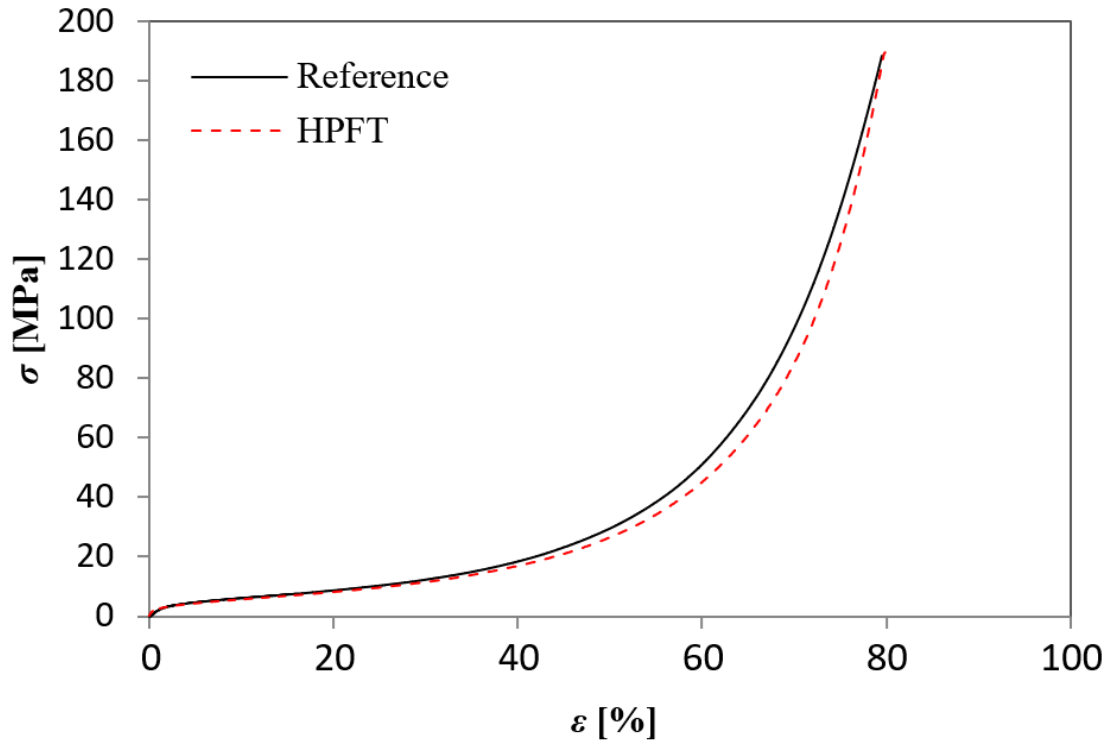


Figure 13. Stress-strain plots of a pore (C) foam tested to HPFT and its reference.

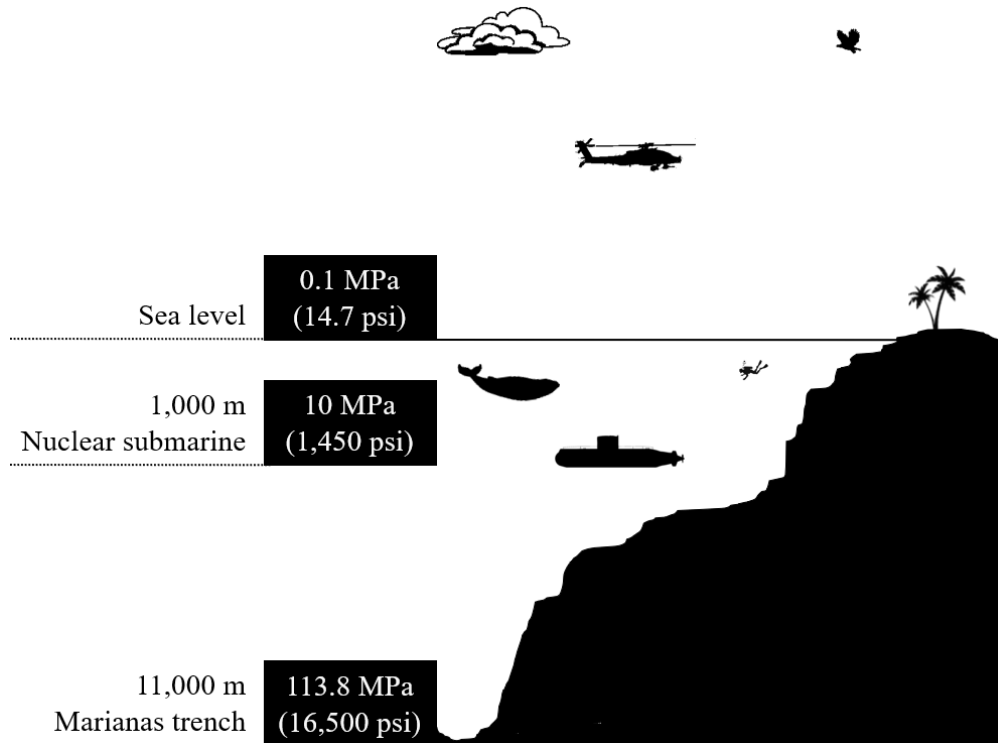


Figure 14. Hydrostatic pressure at different sea levels.

4. Conclusions

The drop of pressure behavior of open-cell Al foams, produced by the replication technique in three different pore sizes, was studied by means of the injection of highly pressurized gasoline additive at pressures up to 172.37 MPa (25,000 psi), at room temperature and 200 °C. According to the physical and geometrical properties of the investigated samples, it was found that a flow rate of $7 \pm 0.2 \text{ cm}^3 \text{ s}^{-1}$ of gasoline additive, the investigated Al foams behaved within the Forchheimer regime. From the high-pressure flow tests at room temperature, it was found that the drop of pressure values tended to be lower as the pore size decreases, contrary to the expected, based on prior research made by other authors. These unexpected outcomes are attributed to the existent inverse correlation between the fluid velocity and the pressure exerted by the fluid. As the highest estimated fluid velocity was reached for the smallest pore (A) it is assumed that the pressure exerted by the fluid toward the foam surface was lower when compared to that for the larger pores (B and C). Thereby, it is thought that the friction between the fluid and the foam surface is lower, as well as the flow resistance. From the high-pressure flow tests (200 °C) it was found that the drop of pressure is more related to the testing temperature than the foam physical and geometrical properties. Thus, it is speculated that the pore size (and therefore, pore-pore interconnections area) influence becomes negligible when the working temperature is high enough ($\geq 200 \text{ °C}$). From visual examination and compression tests, it was determined that open-cell Al foams have the structural capacity to conduct fluids at pressures up to 172.37 MPa and 200 °C, as the studied samples did not exhibit any apparent physical damage or structural collapse. Thus, the functional applicability of this material is expanded to more industries, such as the energy industry.

Acknowledgments

The authors would like to acknowledge the financial support from DGAPA-PAPIIT UNAM "IN102319" for funding the project. C. Flores, G. A. Lara-Rodriguez, A. Tejada, O. Novelo, C. Ramos, R. Reyes, A. Lopez V., F. Garcia, E. de la Calleja and V. Aranda are also acknowledged for their technical support. "Por mi raza hablará el espíritu".

References

- Banhart, J. (2000), Manufacturing Routes for Metallic Foams, *JOM* 52(12), 22-27.
<https://doi.org/10.1007/s11837-000-0062-8>
- Banhart, J. (2001). Manufacture, characterisation and application of cellular metals and metal foams. *Progress in Materials Science*, 46(6), 559–632.
[https://doi.org/10.1016/S0079-6425\(00\)00002-5](https://doi.org/10.1016/S0079-6425(00)00002-5)
- Besser, M. F., & Eisenhammer, T. (1997). Deposition and Applications of Quasicrystalline Coatings. *MRS Bulletin*, 22(11), 59–63.
<https://doi.org/10.1557/S088376940003445X>
- Blick, E. F., & Civan, F. (1988). Porous-Media Momentum Equation for Highly Accelerated Flow. *SPE Reservoir Engineering*, 3(03), 1048–1052.
<https://doi.org/10.2118/16202-PA>
- Boomsma, K., & Poulikakos, D. (2002). The Effects of Compression and Pore Size Variations on the Liquid Flow Characteristics in Metal Foams. *Journal of Fluids Engineering*, 124(1), 263–272.
<https://doi.org/10.1115/1.1429637>
- Chilton, T. H., & Colburn, A. P. (1931). II—pressure drop in packed tubes. *Industrial & Engineering Chemistry*, 23(8), 913-919.
<https://doi.org/10.1021/ie50260a016>
- Despois, J. F., & Mortensen, A. (2005). Permeability of open-pore microcellular materials. *Acta materialia*, 53(5), 1381-1388.
<https://doi.org/10.1016/j.actamat.2004.11.031>
- Despois, J. F., Marmottant, A., Salvo, L., & Mortensen, A. (2007). Influence of the infiltration pressure on the structure and properties of replicated aluminium foams. *Materials Science and Engineering: A*, 462(1-2), 68-75.
<https://doi.org/10.1016/j.msea.2006.03.157>
- Dietrich, B. (2012). Pressure drop correlation for ceramic and metal sponges. *Chemical engineering science*, 74, 192-199.
<https://doi.org/10.1016/j.ces.2012.02.047>

- Dubois, J. M. (2012). Properties and applications of quasicrystals and complex metallic alloys. *Chemical Society Reviews*, 41(20), 6760-6777.
<https://doi.org/10.1039/c2cs35110b>
- Dukhan, N. (2012). Analysis of Brinkman-extended Darcy flow in porous media and experimental verification using metal foam. *Journal of fluids engineering*, 134(7).
<https://doi.org/10.1115/1.4005678>
- Dukhan, N., & Ali, M. (2012). Effect of confining wall on properties of gas flow through metal foam: an experimental study. *Transport in porous media*, 91(1), 225-237.
<https://doi.org/10.1007/s11242-011-9841-7>
- Dukhan, N., Bağcı, Ö., & Özdemir, M. (2014). Metal foam hydrodynamics: Flow regimes from pre-Darcy to turbulent. *International Journal of Heat and Mass Transfer*, 77, 114-123.
<https://doi.org/10.1016/j.ijheatmasstransfer.2014.05.017>
- Fernández-Morales, P., Cano-Montoya, C. A., Pérez-Mesa, J. A., & Navacerrada, M. Á. (2016). Thermal and permeability properties of metal aluminum foams for functional applications. *Ingeniería y Universidad*, 21(1).
<https://doi.org/10.11144/Javeriana.iyu21-1.tppm>
- García-Moreno, F. (2016). Commercial Applications of Metal Foams: Their Properties and Production, *Materials* 9, 85 -111.
<https://doi.org/10.3390/ma9020085>
- Gibson, L. J. & Ashby, M. F. (1997). Cellular Solids: Structure and Properties. *Press Syndicate of the University of Cambridge, Cambridge, UK*, 175-231.
<https://doi.org/10.1017/CBO9781139878326>
- Grossmann, S., Siewert, S., Ott, R., Schmitz, K.-P., Kohse, S., Schmidt, W., & Grabow, N. (2018). Standardized technique of water permeability measurement for biomedical applications. *Current Directions in Biomedical Engineering*, 4(1), 633-636.
<https://doi.org/10.1515/cdbme-2018-0152>
- Luna, E. M. E., Barari, F., Woolley, R., & Goodall, R. (2014). Casting protocols for the production of open cell aluminum foams by the replication technique and the effect on porosity. *Journal of Visualized Experiments*, 94.
<https://doi.org/10.3791/52268>
- Lefebvre, L. P., Banhart, J., & Dunand, D. C. (2008). Porous metals and metallic foams: current status and recent developments. *Advanced engineering materials*, 10(9), 775-787.
<https://doi.org/10.1002/adem.200800241>
- Liu, P. S. & Chen, G. F. (2014) *Porous Materials: Processing and Applications*, Butterworth-Heinemann, pp. 1-188.
- Mancin, S., Zilio, C., Cavallini, A., & Rossetto, L. (2010). Pressure drop during air flow in aluminum foams. *International Journal of Heat and Mass Transfer*, 53(15-16), 3121-3130.
<https://doi.org/10.1016/j.ijheatmasstransfer.2010.03.015>
- Osorio-Hernández, J. O., Suarez, M. A., Goodall, R., Lara-Rodriguez, G. A., Alfonso, I., & Figueroa, I. A. (2014). Manufacturing of open-cell Mg foams by replication process and mechanical properties. *Materials & Design*, 64, 136-141.
<https://doi.org/10.1016/j.matdes.2014.07.015>
- Otaru, A. J., Morvan, H. P., & Kennedy, A. R. (2018). Measurement and simulation of pressure drop across replicated porous aluminium in the Darcy-Forchheimer regime. *Acta Materialia*, 149, 265-273.
<https://doi.org/10.1016/j.actamat.2018.02.051>
- Otaru, A. J. (2019). Review on processing and fluid transport in porous metals with a focus on bottleneck structures. *Metals and Materials International*, 26, 510-525.
<https://doi.org/10.1007/s12540-019-00345-9>
- Pal, L., Joyce, M. K., & Fleming, P. D. (2006). A simple method for calculation of the permeability coefficient of porous media. *Tappi Journal*, 5(9), 10.
- San Marchi, C. & Mortensen, A. (2002) *Infiltration and the Replication Process for Producing Metal Sponges*, in: Degischer, H.P. and Kriszt, B. (eds.) *Handbook of Cellular Metals: Production, Processing, Applications*, Wiley-VCH, pp. 43-56.
- Shi, T., Chen, X., Cheng, Y., & Li, Y. (2017). Foaming process and properties of 6063 aluminum foams by melt foaming method. *Materials Transactions*, 58, 243-248.
<https://doi.org/10.2320/matertrans.M2016244>
- Suarez, M. A., Figueroa, I. A., Gonzalez, G., Lara-Rodriguez, G. A., Novelo-Peralta, O., Alfonso, I., & Calvo, I. J. (2014). Production of Al-Cu-Fe metallic foams without foaming agents or space holders. *Journal of alloys and compounds*, 585, 318-324.
<https://doi.org/10.1016/j.jallcom.2013.08.015>
- Tiab, D. & Donaldson, E. C. (2012) *Petrophysics: Theory and Practice of Measuring Reservoir Rocks and Fluid Transport Properties*, Waltham, MA, USA: Gulf Professional Publishing, pp. 85-125.

Trinidad, J., Marco, I., Arruebarrena, G., Wendt, J., Letzig, D., Sáenz de Argandoña, E., & Goodall, R. (2014). Processing of magnesium porous structures by infiltration casting for biomedical applications. *Advanced Engineering Materials*, 16(2), 241-247.
<https://doi.org/10.1002/adem.201300236>

Velasco-Castro, M., Figueroa, I. A., Pfeiffer, H., & Gómez-García, J. F. (2018). Enhanced CO₂ capture capacity on open-cell Mg foams via humid impregnation with lithium at low temperatures. *Thermochimica Acta*, 664, 73-80.
<https://doi.org/10.1016/j.tca.2018.04.009>

Zeng, Z., & Grigg, R. (2006). A criterion for non-Darcy flow in porous media. *Transport in porous media*, 63(1), 57-69.
<https://doi.org/10.1007/s11242-005-2720-3>